

Moving spiral wave chimeras

Martin Bataille-Gonzalez ¹, Marcel G. Clerc ¹, and Oleh E. Omel'chenko ^{2,*}

¹*Departamento de Física and Millenium Institute for Research in Optics, Facultad de Ciencias Físicas y Matemáticas, Universidad de Chile, Casilla 487-3, Santiago, Chile*

²*Institute of Physics and Astronomy, University of Potsdam, Karl-Liebknecht-Straße 24/25, 14476 Potsdam, Germany*



(Received 29 March 2021; accepted 4 August 2021; published 20 August 2021)

We consider a two-dimensional array of heterogeneous nonlocally coupled phase oscillators on a flat torus and study the bound states of two counter-rotating spiral chimeras, shortly two-core spiral chimeras, observed in this system. In contrast to other known spiral chimeras with motionless incoherent cores, the two-core spiral chimeras typically show a drift motion. Due to this drift, their incoherent cores become spatially modulated and develop specific fingerprint patterns of varying synchrony levels. In the continuum limit of infinitely many oscillators, the two-core spiral chimeras can be studied using the Ott-Antonsen equation. Numerical analysis of this equation allows us to reveal the stability region of different spiral chimeras, which we group into three main classes—symmetric, asymmetric, and meandering spiral chimeras.

DOI: [10.1103/PhysRevE.104.L022203](https://doi.org/10.1103/PhysRevE.104.L022203)

Spiral waves are ubiquitous in nature [1]. They can be found in various biological and chemical systems, including cardiac [2] and epithelial [3] tissues, mammalian neocortex [4,5], spatially distributed cell populations [6,7], and oscillatory chemical reactions [8–12]. From a functional point of view, rotating spiral waves are often associated with cardiac arrhythmia and fibrillation [13]. Moreover, such waves have also been observed in two-dimensional cilia arrays [14,15], where they may be related to the transport function of the corresponding tissue or cell colony [16].

Until recently, the mathematical description of spiral waves was mainly based on multicomponent reaction-diffusion systems [17,18] with excitable or oscillatory local dynamics. The effect of diffusion, in this case, guarantees that the spiral wave profile is smooth everywhere, except the phase defect at the tip of the spiral arms. However, is this a correct assumption for biological systems that consist of individual cells and are therefore inherently discrete? In general, these systems can show more complicated dynamical patterns that differ qualitatively from those in continuous media. A wide variety of such unusual patterns has been recently discovered in systems with nonlocal coupling [19–22]. For example, in 2003, Kuramoto and Shima reported the existence of strange spiral waves in two-dimensional arrays of nonlocally coupled limit-cycle oscillators [23,24]. The spiral arms of these waves consist of synchronized/coherent oscillators and resemble the spiral arms of usual spiral waves in continuous media. But the dynamics of the oscillators close to the spiral defect (in the so called spiral core) turns out to be spatially randomized and incoherent such that it masks the position of the phase defect. Similar coexistence of coherent and incoherent dynamics in a homogeneous oscillatory medium is currently known as the *chimera state* (see Refs. [19–22] and references

therein), therefore spiral waves with coherent spiral arms and incoherent cores were called *spiral wave chimeras* [25] or simply *spiral chimeras*.

So far, spiral chimeras have been observed as motionless patterns with fixed positions of their incoherent cores and uniformly rotating coherent spiral arms. In particular, one-core and multicore spiral chimeras were reported in two-dimensional arrays with open boundary conditions [23–25] and periodic boundary conditions representing a flat torus [26–31] or a sphere [32,33]. Beyond phase oscillator models, the existence of spiral chimeras was also confirmed for many realistic systems consisting of limit-cycle oscillators [23,24,34–38], integrate-and-fire neurons [39,40], or even locally chaotic dynamical units [41]. Moreover, recently spiral chimeras were observed in laboratory experiments with the discrete Belousov-Zhabotinsky (BZ) chemical oscillators [42–44].

In this Letter, we show that spiral wave chimeras, in general, do not need to be motionless. Even in translationally invariant systems with isotropic nonlocal coupling, they can move along straight lines or more complicated twisted trajectories. Similarly to moving spiral pairs in oscillatory continuous media [45], the simplest moving spiral chimera looks like a bound state of two reflection-symmetric counter-rotating spirals that move perpendicular to the line connecting their cores. However, due to nonlocal coupling, these chimera states acquire several remarkable properties. First, their core regions are typically spatially modulated. Second, the symmetry breaking in spiral chimeras occurs quite differently than in continuous media [46,47]: Even if the two spiral cores are nonidentical, they continue to drift together. Moreover, in some cases, the direction of the chimera's movement turns out to depend smoothly on system parameters. As a result, asymmetric spiral chimeras can move in arbitrary direction, even along the line connecting their cores.

*Corresponding author: omelchenko@uni-potsdam.de

Model. We consider a two-dimensional array of phase oscillators $\{\theta_{jk}(t)\}_{j,k=1}^N$ evolving according to

$$\frac{d\theta_{jk}}{dt} = \omega_{jk} - \frac{1}{|B_\sigma(j, k)|} \sum_{(m,n) \in B_\sigma(j,k)} \sin(\theta_{jk} - \theta_{mn} + \alpha). \quad (1)$$

Here ω_{jk} are natural frequencies of the oscillators drawn randomly and independently from a Lorentzian distribution $g(\omega) = \gamma/[\pi(\omega^2 + \gamma^2)]$, with width $\gamma > 0$, $\alpha \in (0, \pi/2)$ is the phase lag parameter, $\sigma \in (0, 1/2)$ is the relative coupling radius, and

$$B_\sigma(j, k) = \{(m, n) : (m - j)^2 + (n - k)^2 \leq \sigma^2 N^2\}$$

denotes the circular neighborhood of the point (j, k) where the distances $m - j$ and $n - k$ are considered mod N . The interaction term in Eq. (1) is referred to as nonlocal coupling and is normalized by the number of points $|B_\sigma(j, k)|$ in the neighborhood $B_\sigma(j, k)$.

It is well known [30] that Eq. (1) supports different motionless chimera patterns, including stripe and spot chimera states as well as four-core spiral chimeras. This Letter demonstrates that the same equation also supports a qualitatively different type of chimera states, called *moving spiral chimeras*. Figure 1 provides several examples of such states in the array of 1024×1024 oscillators (see also Ref. [48] for their movies). The left column shows the phase snapshots, while the right column shows the corresponding local order parameters calculated by

$$z_{jk}(t) = \frac{1}{|B_\delta(j, k)|} \sum_{(m,n) \in B_\delta(j,k)} e^{i\theta_{mn}(t)}, \quad (2)$$

with $\delta = 1/(2\sqrt{N})$. By definition, the absolute value $|z_{jk}(t)|$ measures the degree of synchronization between the neighbors of the oscillator $\theta_{jk}(t)$. In particular, $|z_{jk}(t)| = 1$ corresponds to perfect synchrony of the phases, whereas $|z_{jk}(t)| \approx 0$ stands for their complete disorder. Thus a chimera state is characterized by the coexistence of nearly unit values $|z_{jk}(t)|$ in the coherent region with relatively small values of $|z_{jk}(t)|$ in the incoherent region. Notice that to find the positions of incoherent cores it is convenient to use not the local order parameter $z_{jk}(t)$, but a mean field $w_{jk}(t)$ computed by the formula (2) with $\delta = \sigma$. The modulus $|w_{jk}(t)|$ has pronounced minima at the sites, which can be identified with the phase defects of the corresponding spirals.

In our numerical simulations performed with a fixed-step fourth order Runge-Kutta integrator, we have observed three main types of moving two-core spiral chimeras:

(a) Symmetric spiral chimeras. These chimeras have incoherent cores of nearly the same shape and size. In the graph of the local order parameter $z_{jk}(t)$ each incoherent core looks either as a circle with a phase defect in the middle, or as a specific fingerprint pattern composed of curved stripes corresponding to higher and lower local synchrony of the oscillators. Symmetric spiral chimeras move strictly vertically or horizontally.

(b) Asymmetric spiral chimeras. These chimeras have incoherent cores of different shapes and sizes. The cores move

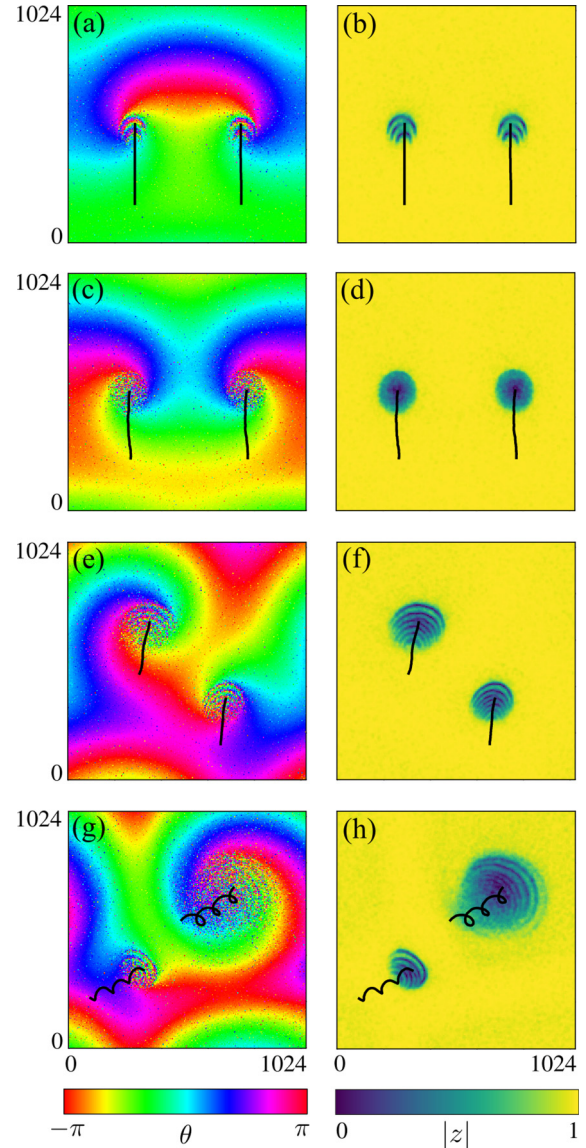


FIG. 1. Moving spiral chimeras in Eq. (1) with $\alpha = 0.6$ [(a) and (b)], $\alpha = 0.7$ [(c) and (d)], $\alpha = 0.8$ [(e) and (f)], and $\alpha = 1.01$ [(g) and (h)]. Other parameters: $N = 1024$, $\sigma = 0.25$, and $\gamma = 0.01$. The left and right columns show snapshots $\theta_{jk}(t)$ and the local order parameters $|z_{jk}(t)|$ computed by (2). The black curves show movement trajectories of the incoherent cores.

along straight lines in a direction, which in general is neither vertical nor horizontal.

(c) Meandering spiral chimeras. These are nonstationary versions of asymmetric spiral chimeras. They move not as a rigid body but rather as a periodically breathing pattern. Their movement trajectories are not straight lines, but twisted curves which can be thought of as a superposition of a uniform drift and oscillatory motion.

In the following, we outline the stability regions in the parameter plane (α, σ) for each of the above moving spiral chimeras.

Methods. For every trajectory of Eq. (1), we can define a piecewise-linear function $Z_N(x, y, t)$ on the flat torus $(x, y) \in$

$[-\pi, \pi]^2$ such that

$$Z_N(-\pi + 2\pi j/N, -\pi + 2\pi k/N, t) = z_{jk}(t).$$

It is well known that in the continuum limit case, i.e., when $N \rightarrow \infty$, the long-term dynamics of $Z_N(x, y, t)$ is asymptotically close to a solution $z(x, y, t)$ of the Ott-Antonsen equation

$$\frac{dz}{dt} = -\gamma z + \frac{1}{2} e^{-i\alpha} \mathcal{G}z - \frac{1}{2} e^{i\alpha} z^2 \mathcal{G}\bar{z}, \quad (3)$$

where \bar{z} denotes the complex conjugate of z , and $\mathcal{G}z$ is a convolution term of the form

$$(\mathcal{G}z)(x, y, t) = \frac{1}{\pi^3 \sigma^2} \iint_{|x-x'|^2 + |y-y'|^2 \leq \pi^2 \sigma^2} z(x', y', t) dx' dy'.$$

Note that the distance $|x - x'|^2 + |y - y'|^2$ in the above integral has to be computed accounting for periodic boundary conditions in the x and y directions. The derivation of Eq. (3) is based on the invariant manifold reduction technique suggested in Ref. [49] and its details can be found in Refs. [21,50]. Thus, the existence and stability of moving spiral chimeras in Eq. (1) can be studied using Eq. (3).

We discretize Eq. (3) on a uniform grid with 256×256 nodes, replace all integrals by trapezoid rule and carry out direct numerical simulations of the resulting ordinary differential equations using the Python *RK45* solver from the SciPy package with adaptive or fixed ($dt = 0.1$) time step. We keep $\gamma = 0.01$ fixed and change parameters σ and α . For every chosen pair (α, σ) we integrate the discretized version of Eq. (3) over 2×10^4 time units. The initial part of the trajectory of the length 10^4 is discarded as a transient and the remaining part of the length 10^4 is analyzed in the following way.

We compute a mean field $w(x, y, t) = (\mathcal{G}z)(x, y, t)$. In the case of a two-core spiral chimera, this complex function has exactly two phase defects where $|w(x, y, t)| = 0$. This allows us to trace the trajectory of each defect and compute its instantaneous velocity $\mathbf{v}(t) = (v_x(t), v_y(t))$. Though the trajectories of two phase defects can be different, the long-time averages $\langle v_x \rangle$ and $\langle v_y \rangle$ calculated along one of the trajectories are the same as those calculated along the other trajectory, therefore we can define two scalars characterizing the spiral chimera motion:

- (i) the mean drift velocity $s = |\langle v_x \rangle + i \langle v_y \rangle|$, and
- (ii) the direction of drift motion

$$\psi = \arg(\langle v_x \rangle + i \langle v_y \rangle).$$

Obviously, for a symmetric spiral chimera, we must obtain $\psi = 0, \pm\pi/2, \pi$, whereas all other values ψ are indications of asymmetric spiral chimeras.

It turns out that all solutions of Eq. (3) corresponding to two-core spiral chimeras assume one of the following two forms. Symmetric and asymmetric spiral chimeras are described by an ansatz

$$z(x, y, t) = a(x - s_x t, y - s_y t) e^{i\Omega t}, \quad (4)$$

where $a(x, y)$ is a complex amplitude and s_x, s_y , and Ω are real constants. A symmetric spiral chimera is obtained if $s_x = 0$ and $a(-x, y) = a(x, y)$ or if $s_y = 0$ and $a(x, -y) =$

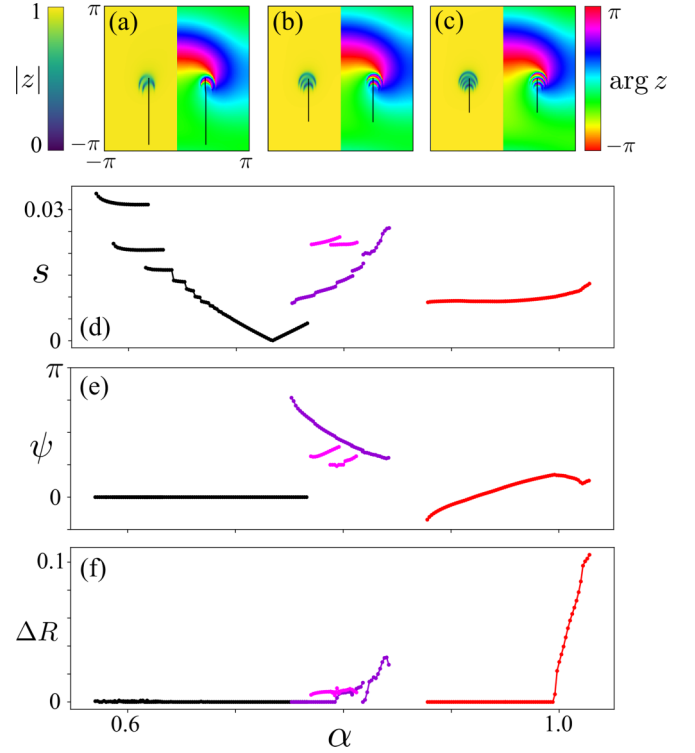


FIG. 2. Mean drift velocity s (d), direction of drift motion ψ (e) and variance of the global order parameter ΔR (f) for two-core spiral chimeras in Eq. (3) with $\sigma = 0.25$ and $\gamma = 0.01$. The black and color dots in (d)–(f) correspond to symmetric and asymmetric spiral chimeras, respectively. Three top panels exemplify solutions $z(x, y, t)$ for $\alpha = 0.58$ (a), $\alpha = 0.60$ (b), and $\alpha = 0.63$ (c). The black curves in these panels show the trajectories of incoherent cores.

$a(x, y)$. Otherwise the spiral chimera is asymmetric. The second ansatz representing meandering spiral chimeras reads

$$z(x, y, t) = a(x - s_x t, y - s_y t) e^{i\Omega t}, \quad (5)$$

where the amplitude $a(x, y, t)$ depends explicitly on time. (Typically this dependence is periodic.) In order to distinguish between cases (4) and (5) numerically one can compute the difference $\Delta R = \max_t R(t) - \min_t R(t)$, where

$$R(t) = \left| \frac{1}{4\pi^2} \int_{-\pi}^{\pi} \int_{-\pi}^{\pi} z(x, y, t) dx dy \right|$$

is the global order parameter. Then in the former case, one obtains $\Delta R = 0$, while in the latter case one gets $\Delta R > 0$. Therefore spiral chimeras described by formulas (4) and (5) can be called stationary and nonstationary spiral chimeras, respectively.

Results. Using the local order parameters from Fig. 1 as initial conditions and performing forward and backward α -sweeps with the step $d\alpha = 0.002$ for fixed coupling radius $\sigma = 0.25$, we obtained a diagram shown in Fig. 2. Note that two adjacent points were connected by a line only in the case if the right point was obtained in the forward sweep starting from the left point and vice versa. Moreover, each sweep was stopped at the value α for which stable two-core spiral chimeras ceased to exist. Figure 2 reveals that stable symmetric spiral chimeras can be found for $\alpha \in$

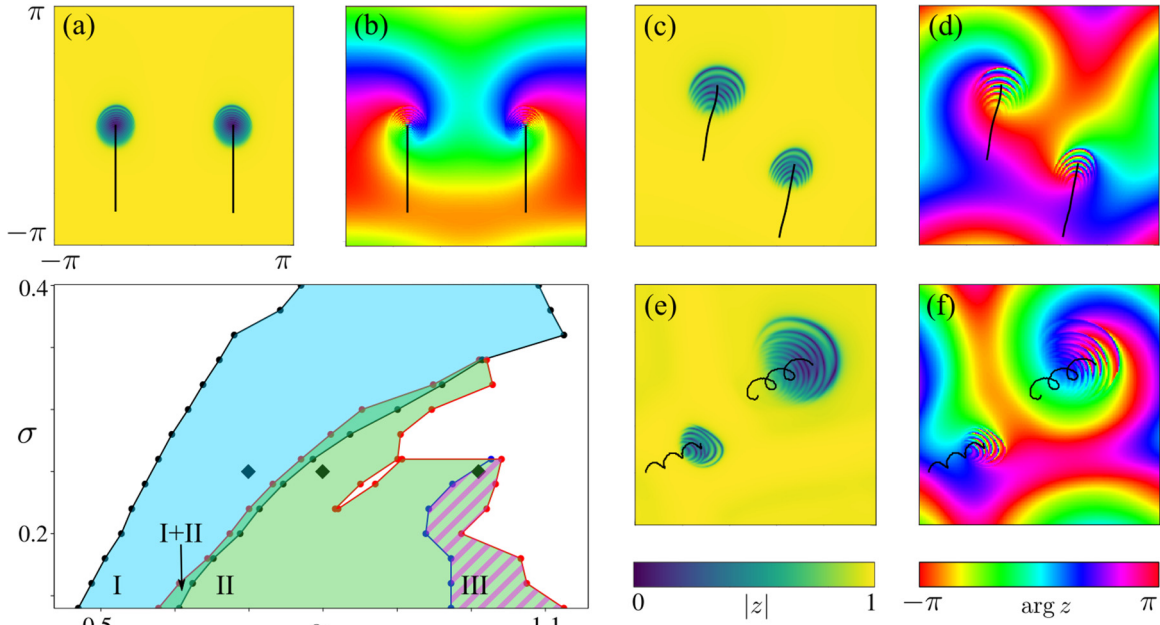


FIG. 3. The main panel (bottom left) shows the stability regions of the symmetric (I), stationary asymmetric (II), and meandering (III) two-core spiral chimeras in the Eq. (3) with $\gamma = 0.01$. The boundaries of these regions consist of the dots, for which α sweeps were carried out, and the interpolating lines. Additional panels exemplify solutions $z(x, y, t)$ for $(\alpha, \sigma) = (0.7, 0.25)$ [(a) and (b)], $(0.8, 0.25)$ [(c) and (d)], and $(1.01, 0.25)$ [(e) and (f)]. These parameters are indicated by diamonds in the stability diagram. The black curves in the panels (a)–(f) show movement trajectories of the incoherent cores.

[0.57, 0.766], whereas stable asymmetric spiral chimeras can be found in two disjoint intervals $\alpha \in [0.752, 0.852]$ and $\alpha \in [0.878, 1.028]$. Note that the ranges of symmetric and asymmetric chimeras have a small overlap where both of them coexist stably. Moreover, several other bi- and tristability ranges can be found in the left and middle parts of the diagram.

The branch of symmetric spiral chimeras consists of several disconnected curves. The chimeras on the leftmost curve are the fastest. Their core regions are simple patterns consisting of two curved stripes corresponding to small values of $|z(x, y, t)|$. On the second and third curves from above we find spiral chimeras with core regions composed of three and four stripes, respectively. The general rule is that for α increasing from 0.57 to 0.734 the motion of spiral chimeras slows down, while the number of stripes in their core regions grows. As a result, these regions begin to look as intricate fingerprint patterns. However, for $\alpha \approx 0.734$ the incoherent stripes merge together and the core regions become circular-shaped, which is typical for motionless spiral chimeras [27].

The branch of asymmetric spiral chimeras also consists of several disconnected curves. All these spiral chimeras have nonvanishing mean velocities $s > 0.008$ and their core regions typically look as fingerprint patterns composed of many incoherent stripes. The most prominent feature of asymmetric spiral chimeras is that for sufficiently large values α they become nonstationary and transform into meandering spiral chimeras. For example, Fig. 2 indicates that asymmetric spiral chimeras are stationary ($\Delta R = 0$) for $\alpha \in [0.752, 0.792]$ (on the slowest part of the branch only) and for $\alpha \in [0.996, 1.028]$. For all other

phase lags these chimeras do not behave as rigidly moving patterns, but breathe periodically on top of the uniform drift motion.

Parameter sweeps similar to Fig. 2 were also performed for other coupling radii σ varying from 0.14 to 0.4 with the step $d\sigma = 0.02$. Thus we obtained a stability diagram shown in Fig. 3. Our general observations can be summarized as follows. The branch of symmetric spiral chimeras has a similar shape for all values σ , though it shifts to larger values α for increasing coupling radius. Regarding the asymmetric spiral chimeras, we found that their stability range has the maximal size for small values σ and shrinks gradually for increasing coupling radius until it eventually vanishes for $\sigma > 0.34$. We also found that the size of the core region of a spiral chimeras typically increases with increasing parameters α and σ . However, the mean drift velocity s turns out to be more sensitive to the changes of the coupling radius σ than to the changes of the phase lag α . Notice that two-core spiral chimeras can also be found for coupling radii smaller than 0.14, but in this case their drift velocity decreases significantly and almost vanishes for $\sigma \leq 0.1$ such that they appear as pinned spiral waves or spiral waves moving along closed circular orbits.

Conclusions. Discrete two-dimensional media made up of oscillatory or excitable active units are found in many biological systems. Above, we have shown that under the influence of nonlocal coupling, these media can support moving spiral wave chimeras with a complex distribution of synchronous and asynchronous regions. Using the Ott-Antonsen equation (3), we computed stability diagrams for these chimera states and found how the speed and the direction of their

drift depend on system parameters. This information can be used to search for moving spiral chimeras in experiments similar to Refs. [42–44] or in the cilia carpet system studied theoretically in Ref. [14].

Several interesting questions about the nature of moving spiral chimeras still remain open. First, it seems likely that the distinct solution curves in Fig. 2 are connected by unstable solution branches. Moreover, it is unclear whether there is a branch that connects the moving spiral chimeras with their motionless counterparts. To answer these questions, one needs to perform a more detailed analysis of traveling wave solutions (4) in Eq. (3) by analogy with Refs. [51,52]. The same approach can also be used to study the behavior of moving spiral chimeras for small values of the coupling radius σ , which we have not addressed in this Letter. Another challenging problem is the rigorous mathematical description of moving spiral chimeras in Eq. (1) with identical oscillators. It is known [53,54] that in this case, Eq. (3) becomes singular and can no longer be used. Finally, we emphasize that Eq. (1) can show more complex moving spiral chimeras, see Fig. 4, which also deserve consideration. We hope that further research in the field will answer the above questions and, therefore,

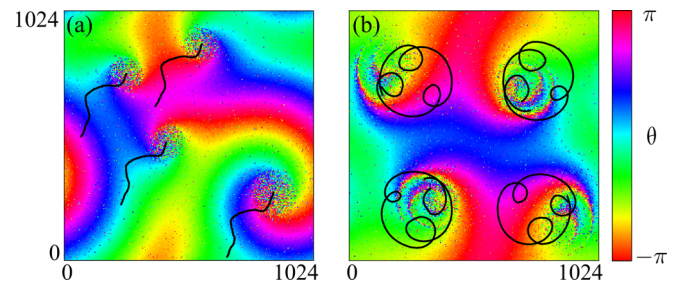


FIG. 4. Four-core moving spiral chimeras in Eq. (1) with $\alpha = 0.8$, $\sigma = 0.2$ (a) and $\alpha = 0.9$, $\sigma = 0.25$ (b). For other parameters and notations see Fig. 1.

improve our understanding of pattern formation in discrete active media with nonlocal coupling.

Acknowledgment. The work of O.E.O. was supported by the Deutsche Forschungsgemeinschaft under Grant No. OM 99/2-1. M.B.G. acknowledges the hospitality of the University of Potsdam during his research internship. M.G.C. thanks for the financial support ANID-Millennium Science Initiative Program–ICN17_012.

- [1] K. Tsuji and S. C. Müller (eds.), *Spirals and Vortices* (Springer, Cham, 2019).
- [2] J. M. Davidenko, A. M. Pertsov, R. Salomonsz, W. Baxter, and J. Jalife, *Nature (London)* **355**, 349 (1992).
- [3] G. Seiden and S. Curland, *New J. Phys.* **17**, 033049 (2015).
- [4] X. Huang, W. C. Troy, Q. Yang, H. Ma, C. R. Laing, S. J. Schiff, and J.-Y. Wu, *J. Neurosci.* **24**, 9897 (2004).
- [5] X. Huang, W. Xu, J. Liang, K. Takagaki, X. Gao, and J.-Y. Wu, *Neuron* **68**, 978 (2010).
- [6] J. Lechleiter, S. Girard, E. Peralta, and D. Clapham, *Science* **252**, 123 (1997).
- [7] J. Lauzeral, J. Halloy, and A. Goldbeter, *Proc. Natl. Acad. Sci. USA* **94**, 9153 (1997).
- [8] A. M. Zhabotinsky and A. N. Zaikin, *J. Theor. Biol.* **40**, 45 (1973).
- [9] A. T. Winfree, *Science* **175**, 634 (1972).
- [10] A. S. Mikhailov and K. Showalter, *Phys. Rep.* **425**, 79 (2006).
- [11] V. K. Vanag and I. R. Epstein, in *Self-Organized Morphology in Nanostructured Materials*, edited by K. Al-Shamery and J. Parisi (Springer, Berlin, 2008), pp. 89–113.
- [12] G. Ertl, *Science* **254**, 1750 (1991).
- [13] R. A. Gray, A. M. Pertsov, and J. Jalife, *Nature (London)* **392**, 75 (1998).
- [14] N. Uchida and R. Golestanian, *Phys. Rev. Lett.* **104**, 178103 (2010).
- [15] R. Golestanian, J. M. Yeomans, and N. Uchida, *Soft Matter* **7**, 3074 (2011).
- [16] W. Gilpin, M. S. Bull, and M. Prakash, *Nat. Rev. Phys.* **2**, 74 (2020).
- [17] A. T. Winfree, *Chaos* **1**, 303 (1991).
- [18] D. Barkley, *Phys. Rev. Lett.* **72**, 164 (1994).
- [19] M. J. Panaggio and D. M. Abrams, *Nonlinearity* **28**, R67 (2015).
- [20] E. Schöll, *Eur. Phys. J. Spec. Top.* **225**, 891 (2016).
- [21] O. E. Omel’chenko, *Nonlinearity* **31**, R121 (2018).
- [22] S. Majhi, B. K. Bera, D. Ghosh, and M. Perc, *Phys. Life Rev.* **28**, 100 (2019).
- [23] Y. Kuramoto and S. Shima, *Prog. Theor. Phys. Suppl.* **150**, 115 (2003).
- [24] S. I. Shima and Y. Kuramoto, *Phys. Rev. E* **69**, 036213 (2004).
- [25] E. A. Martens, C. R. Laing, and S. H. Strogatz, *Phys. Rev. Lett.* **104**, 044101 (2010).
- [26] P.-J. Kim, T.-W. Ko, H. Jeong, and H.-T. Moon, *Phys. Rev. E* **70**, 065201(R) (2004).
- [27] O. E. Omel’chenko, M. Wolfrum, S. Yanchuk, Y. L. Maistrenko, and O. Sudakov, *Phys. Rev. E* **85**, 036210 (2012).
- [28] M. J. Panaggio and D. M. Abrams, *Phys. Rev. Lett.* **110**, 094102 (2013).
- [29] J. Xie, E. Knobloch, and H.-C. Kao, *Phys. Rev. E* **92**, 042921 (2015).
- [30] C. R. Laing, *SIAM J. Appl. Dyn. Syst.* **16**, 974 (2017).
- [31] O. E. Omel’chenko, M. Wolfrum, and E. Knobloch, *SIAM J. Appl. Dyn. Syst.* **17**, 97 (2018).
- [32] M. J. Panaggio and D. M. Abrams, *Phys. Rev. E* **91**, 022909 (2015).
- [33] R.-S. Kim and C.-U. Choe, *Phys. Rev. E* **98**, 042207 (2018).
- [34] X. Tang, T. Yang, I. R. Epstein, Y. Liu, Y. Zhao, and Q. Gao, *J. Chem. Phys.* **141**, 024110 (2014).
- [35] B.-W. Li and H. Dierckx, *Phys. Rev. E* **93**, 020202(R) (2016).
- [36] A. V. Bukh and V. S. Anishchenko, *Chaos Solitons Fract.* **131**, 109492 (2020).
- [37] I. A. Shepelev, A. V. Bukh, S. S. Muni, and V. S. Anishchenko, *Regul. Chaotic Dynam.* **25**, 597 (2020).
- [38] V. Maistrenko, O. Sudakov, and Y. Maistrenko, *Eur. Phys. J. Spec. Top.* **229**, 2327 (2020).
- [39] A. Schmidt, T. Kasimatis, J. Hizanidis, A. Provata, and P. Hövel, *Phys. Rev. E* **95**, 032224 (2017).
- [40] G. Argyropoulos and A. Provata, *Front. Appl. Math. Stat.* **5**, 35 (2019).

- [41] C. Gu, G. St-Yves, and J. Davidsen, *Phys. Rev. Lett.* **111**, 134101 (2013).
- [42] S. Nkomo, M. R. Tinsley, and K. Showalter, *Phys. Rev. Lett.* **110**, 244102 (2013).
- [43] J. F. Tetz, J. Rode, M. R. Tinsley, K. Showalter, and H. Engel, *Nat. Phys.* **14**, 282 (2017).
- [44] J. F. Tetz, M. R. Tinsley, H. Engel, and K. Showalter, *Sci. Rep.* **10**, 7821 (2020).
- [45] I. S. Aranson, L. Kramer, and A. Weber, *Phys. Rev. E* **47**, 3231 (1993).
- [46] I. S. Aranson, L. Kramer, and A. Weber, *Phys. Rev. E* **48**, R9(R) (1993).
- [47] I. Schebesch and H. Engel, *Phys. Rev. E* **60**, 6429 (1999).
- [48] See the Supplemental Material <http://link.aps.org/supplemental/10.1103/PhysRevE.104.L022203> for movies showing the dynamics of spiral wave chimeras in Figs. 1(a), 1(e), and 1(g).
- [49] E. Ott and T. M. Antonsen, *Chaos* **18**, 037113 (2008).
- [50] C. R. Laing, *Physica D* **238**, 1569 (2009).
- [51] O. E. Omel'chenko, *Nonlinearity* **33**, 611 (2020).
- [52] C. R. Laing and O. E. Omel'chenko, *Chaos* **30**, 043117 (2020).
- [53] O. E. Omel'chenko, *J. Phys. A: Math. Theor.* **52**, 104001 (2019).
- [54] J. Xie, E. Knobloch, and H.-C. Kao, *Phys. Rev. E* **90**, 022919 (2014).